Top Catal (2017) 60:492–502
DOI 10.1007/s11244-016-0714-8

ORIGINAL PAPER

Fe Oxides on Ag Surfaces: Structure and Reactivity

M. Shipilin[1] · E. Lundgren[1] · J. Gustafson[1] · C. Zhang[1] · F. Bertram[2] · C. Nicklin[3] · C. J. Heard[4] · H. Grönbeck[4] · F. Zhang[5] · J. Choi[5] · V. Mehar[5] · J. F. Weaver[5] · L. R. Merte[1]

Published online: 9 September 2016

Abstract One layer thick iron oxide films are attractive from both applied and fundamental science perspectives. The structural and chemical properties of these systems can be tuned by changing the substrate, making them promising materials for heterogeneous catalysis. In the present work, we investigate the structure of FeO(111) monolayer films grown on Ag(100) and Ag(111) substrates by means of microscopy and diffraction techniques and compare it with the structure of FeO(111) grown on other substrates reported in literature. We also study the NO adsorption properties of FeO(111)/Ag(100) and FeO(111)/Ag(111) systems utilizing different spectroscopic techniques. We discuss similarities and differences in the data obtained from adsorption experiments and compare it with previous results for FeO(111)/Pt(111).

This article originally listed an author (J. F. Weaver) incorrectly. The article has been updated.

Electronic supplementary material The online version of this article (doi:10.1007/s11244-016-0714-8) contains supplementary material, which is available to authorized users.

✉ M. Shipilin
mikhail.shipilin@sljus.lu.se

[1] Division of Synchrotron Radiation Research, Lund University, Box 118, 221 00 Lund, Sweden

[2] DESY Photon Science, Notkestr. 85, 22607 Hamburg, Germany

[3] Diamond Light Source, OX11 0DE, Didcot, Oxfordshire, UK

[4] Chalmers University of Technology, 412 96 Göteborg, Sweden

[5] Department of Chemical Engineering, University of Florida, Gainesville, FL 32611, USA

Keywords FeO · Ag · Surface X-ray diffraction · Reactivity · Single crystal surfaces · Surface structure

1 Introduction

Ultra-thin metal oxides grown on various substrates have recently attracted increased scientific and technological interest. Due to the oxide—substrate interaction, the structural parameters of such materials are tunable and the systems offer a possibility to study and tailor surface chemical and physical properties. These kinds of novel functional materials have a wide range of applications including heterogeneous catalysis as a prominent example [1–5].

The surface of a metal oxide thin film differs fundamentally from the surface of a pure metal catalyst owing to the presence of both acidic and basic surface sites. The intrinsic availability of oxygen atoms in the material also plays a significant role in e.g., oxidation reactions [6–8]. Ultra-thin iron oxides, in particular, have been shown to be catalytically active in e.g., reactions of selective oxidation and dehydrogenation [9].

Depending on the substrate, preparation conditions, and thickness, iron oxides can grow with different stoichiometry (most common are magnetite (Fe_3O_4), hematite (α-Fe_2O_3) and wüstite FeO), and with different crystallographic orientations of the surface. In the case of non-stoichiometric compounds, iron ions have different coordination and thus different oxidation state while Fe ions in stoichiometric FeO have a single oxidation state. This difference affects the adsorption and reaction properties of the surface.

The FeO stoichiometry is commonly observed for one layer thick films grown on various substrates with both hexagonal [10–14] and square [15–19] symmetry. Intriguingly, in most cases such films grow with an in-plane structure similar to (111) termination of bulk wüstite,

where the surface is unstable due to the polar nature of the (111) termination of this rock-salt-like compound [20]. Even when thicker films with other stoichiometry were studied, the FeO(111) monolayer was reported to precede the formation of a final structure [10, 11, 21–25].

The growth of ultra-thin iron oxide films on Pt(111) was first investigated in the late 80s [26] and since then Pt has been by far the most used and studied substrate. Recently, several groups have shown that a one layer thick FeO(111) layer on Pt(111) exhibits a higher catalytic activity toward low-temperature CO oxidation than platinum itself. For example, Sun and co-workers [27, 28] utilized several experimental techniques including scanning tunneling microscopy (STM), low-energy electron diffraction (LEED), Auger electron spectroscopy (AES) and temperature programmed desorption (TPD) and proposed a reaction mechanism involving the formation of a well-ordered, oxygen rich FeO_x ($1 < x < 2$) film [29] that reacts with CO via a Mars-van Krevelen mechanism. However, in works [30–32] the authors studied the same system using STM and density functional theory (DFT) and concluded that the role of coordinatively unsaturated ferrous (CUF) sites on the edges of FeO islands is important for CO oxidation reaction. The atomic-scale mechanisms of catalytic reactions involving iron oxides are thereby still not entirely clear. To be able to tune the chemical properties of such systems, a full understanding of their structure and interactions with adsorbing molecules is desirable.

In this contribution, we report results of STM, LEED and surface X-ray diffraction (SXRD) structural studies of FeO(111) monolayers grown on Ag(100) and Ag(111) and compare them with data reported in the literature for other substrates. We also show the results of TPD and reflection absorption infrared spectroscopy (RAIRS) experiments aimed to study NO adsorption on the FeO(111) layer to further characterize the surface sites. We show that the NO adsorption properties on FeO(111)/Ag(100) and FeO(111)/Ag(111) are similar despite the difference in the coincidence pattern due to the underlying substrate. Therefore, we conclude that the NO adsorption is determined by the in-plane distance governing the internal rumpling of the O and Fe atoms in the FeO(111) layer. We compare the present observations with results reported for NO adsorption on FeO(111)/Pt(111), in which the FeO(111) in-plane distance is significantly smaller resulting in a higher degree of rumpling and negligible NO adsorption at liquid nitrogen temperatures.

2 Experimental

2.1 Sample Preparation

Before all measurements, the samples were cleaned by cycles of Ar^+ sputtering (1.5 keV energy and 2×10^{-5} mbar gas pressure) and annealing at 500 °C. This procedure was repeated until the LEED pattern (all setups in the present work were equipped with a LEED instrument) indicated a clean Ag surface with the corresponding orientation. Additionally, in the STM experiments we used an Auger spectrometer integrated into the setup, which did not detect any contaminants.

One layer thick films were grown by deposition of iron in the presence of oxygen (reactive physical vapor deposition (RPVD)) using an electron beam evaporator at 100 °C substrate temperature and 2×10^{-7} mbar background O_2 pressure with subsequent annealing to 400 °C in vacuum according to the procedure developed earlier [33]. The evaporators were calibrated with a reference to a Pt(111) crystal, where the density of one monolayer is known (one closed monolayer of FeO(111) on Pt(111) has the density of 1.2×10^{15} cm^{-2} of Fe atoms). The quality of the films was checked by LEED and where possible by AES.

To describe the crystal structure, basis vectors corresponding to the unit cell of respective substrates were used. In the case of the Ag(100) single crystal, the set of mutually perpendicular vectors $\boldsymbol{a}_1^{Ag(100)}$, $\boldsymbol{a}_2^{Ag(100)}$ lying in the surface plane and $\boldsymbol{a}_3^{Ag(100)}$ pointing upwards along the surface normal (a tetragonal basis) was applied. In terms of the bulk lattice constant $\boldsymbol{a}_0$ ($\boldsymbol{a}_0$(Ag) = 4.09 Å) the lengths of these vectors can be expressed as $\left|\boldsymbol{a}_1^{Ag(100)}\right| = \left|\boldsymbol{a}_2^{Ag(100)}\right| = \frac{a_0}{\sqrt{2}} = 2.89$ Å and $\left|\boldsymbol{a}_3^{Ag(100)}\right| = a_0 = 4.09$ Å. The corresponding reciprocal basis is thus also tetragonal, and the lengths of reciprocal lattice vectors are $\left|\boldsymbol{b}_1^{Ag(100)}\right| = \left|\boldsymbol{b}_2^{Ag(100)}\right| = 2.17$ $Å^{-1}$ and $\left|\boldsymbol{b}_3^{Ag(100)}\right| = 1.54$ $Å^{-1}$. These values are referred to as reciprocal lattice units (RLU) for the Ag(100) substrate and FeO films grown on it throughout the work. The crystal basis used to describe FeO films grown on a Ag(111) substrate is a hexagonal basis with vectors $\boldsymbol{a}_1^{Ag(111)}$ and $\boldsymbol{a}_2^{Ag(111)}$ lying in the surface plane with 60° angle between each other and $\boldsymbol{a}_3^{Ag(111)}$ perpendicular to them pointing upwards along the surface normal. The lengths of these vectors are $\left|\boldsymbol{a}_1^{Ag(111)}\right| = \left|\boldsymbol{a}_2^{Ag(111)}\right| = \frac{a_0}{\sqrt{2}} = 2.89$ Å and $\left|\boldsymbol{a}_3^{Ag(111)}\right| = a_0 \cdot \sqrt{3} = 7.08$ Å. The corresponding reciprocal space vectors then are $\left|\boldsymbol{b}_1^{Ag(111)}\right| = \left|\boldsymbol{b}_2^{Ag(111)}\right| = 2.17$ $Å^{-1}$ with 120° angle between them and $\left|\boldsymbol{b}_3^{Ag(111)}\right| = 0.89$ $Å^{-1}$ collinear to $\boldsymbol{a}_3^{Ag(111)}$. These values are used as RLU for the Ag(111) substrate and the films grown on it.

2.2 STM

The microscopy measurements were performed at the Division of Synchrotron Radiation Research at Lund

University, Lund, Sweden. The images were recorded in constant current mode using an Omicron STM1 microscope with an electrochemically etched tungsten tip in a UHV chamber with a base pressure of about 5×10^{-11} mbar. Image treatment included flattening, drift correction and brightness/contrast enhancement. The bias voltages provided in the work are identified with the sample.

2.3 SXRD

Diffraction experiments were performed at the I07 beamline at Diamond Light Source in England for an Ag(100) single crystal. In the present experiments, 18 keV photons were directed at the sample surface under an incident angle of 0.2° (the critical angle of total external reflection for silver at that energy is 0.194°) to achieve high surface sensitivity. The patterns were collected with a Pilatus 100 K area detector. The process of data extraction and treatment has recently been discussed in detail in [34]. All necessary corrections were applied to the obtained values of structure factor (F_{str}) in accordance with the experimental geometry [35, 36]. The fitting of experimental data was performed using the specialized software ROD by Elias Vlieg and WINROD by Daniel Kaminski [37]. The details of fitting process can be found in the supplementary information.

2.4 Theoretical Calculations

Total energy calculations and local geometry optimization were performed with VASP 5.2 [38–41], using the projected augmented wavefunction (PAW) method and plane-waves truncated at 400 eV to expand the Kohn–Sham orbitals. The gradient corrected exchange correlation functional according to Perdew, Burke, and Ernzerhof (PBE) was used [42]. Iron oxide layers were treated within the LDA+U formalism, with U and J parameters of 4 and 1 eV respectively, located on all iron atoms. These values were previously found to provide a satisfactory description of bulk characteristics of FeO [43]. All calculations were performed spin unrestricted. Reciprocal space integration over the Brillouin zone was approximated with finite sampling using Monkhorst–Pack grids [44, 45]. The Methfessel Paxton scheme with a thermal width of 0.1 eV was used to smear the Fermi discontinuity. Local geometry optimization was performed with the BFGS algorithm as implemented in VASP. The structures were considered to be converged when the forces were below 0.01 eV/Å. Ag(100) was modeled with a four layer 2×11 cell, which represents the full experimental unit cell of FeO(111)/Ag(100). The metal support was fixed during the geometry optimization.

Simulations of the STM images were performed within the Tersoff − Hamann approximation [46] and simulated with a negative bias of 1.0 eV.

2.5 TPD and RAIRS

The results reported in the current work were obtained in an ultra-high vacuum (UHV) chamber with a typical base pressure of about 2×10^{-10} mbar [47, 48]. The instrumentation available in the chamber includes a "Hiden" quadrupole mass spectrometer (QMS) for TPD measurements and a "Bruker Tensor 27″ Fourier transform infrared spectrometer (FTIR) for RAIRS measurements (with the resolution set to 4 cm^{-1}).

The crystals used in the present study were mounted on W wires and attached to a copper sample holder cooled with liquid nitrogen. The temperature was measured by a K-type thermocouple clamped to the edge of the samples and controlled using a proportional–integral–derivative (PID) controller.

To perform TPD experiments, we exposed the sample surface to NO at various partial pressures and a substrate temperature of 87–90 K. After exposures we positioned the sample surface in front of the nozzle of the QMS at a distance of about 5 mm and heated at a constant rate of 1 K/s. The spectrometer was set to detect traces of N_2 ($m/z = 28$), NO ($m/z = 30$), N_2O ($m/z = 44$) and NO_2 ($m/z = 46$). During TPD, we detected insignificant amounts of N_2, N_2O and NO_2 mainly in the low temperature region of about 100 K, which was attributed to the process of decomposition of adsorbed NO dimers – analogous to behavior observed previously on Ag surfaces [49–51]. At higher temperatures, a reversible adsorption/desorption of NO molecules was observed.

We considered the saturation coverage of NO to be reached when an NO molecule was adsorbed on each Fe cation of the FeO(111) monolayer. This consideration was found to be reasonable for NO adsorbed on an FeO(111) monolayer grown on Ag(100) [52]. The estimated accuracy of the NO coverages in the experiments reported here lies within about 15 %. Test experiments were performed for clean surfaces showing no NO adsorption.

3 Results

One layer thick FeO films were grown on Ag(100) and Ag(111) single crystals. Different submonolayer surface coverages (not shown here) could be produced, depending on the deposition time. On both substrates films start to grow as flat islands wetting the surface and merging together upon increase of the deposition time. In the

current work the surface coverage of ~0.4 monolayer on both substrates is discussed. According to STM data, the distribution of the size of islands on both surfaces in this case is rather broad with the average of about 50 × 30 nm on Ag(100) where the islands have an irregular oval shape elongated along {011} directions of the substrate and about 30 nm in diameter on Ag(111) where the islands tend to have a regular hexagonal shape.

3.1 In-Plane Geometry

Figure 1a, b shows atomically resolved STM images and LEED patterns of FeO(111)/Ag(100) and FeO(111)/Ag(111) respectively. The LEED patterns in both cases exhibit reflections belonging to the substrate unit cell (black dashed lines), the FeO(111) unit cell and the coincidence structure (green and white diamonds in both the STM and LEED images).

The FeO on Ag(100) structure exhibits a quasi-hexagonal atomic arrangement with a lattice parameter of about 3 Å corresponding to the (111) crystallographic orientation. A longer-range periodicity is observed along the [011] and [0-11] crystallographic directions of the substrate forming $(2 \times x)$ type of superstructure. Merte et al. [33] have shown that a FeO(111) layer grows on a Ag(100) surface with a varying coincidence periodicity, which on average can be represented as two types of coincidence structure, namely $p(2 \times 11)$ and $c(2 \times 12)$ structures (see Fig. 2a) resulting in a mean Fe–Fe spacing of 3.25–3.26 Å. The corresponding surface concentration of Fe cations is equal to ~91 % of the surface atom density of the Ag(100) substrate. Because the LEED instrument was not optimized for fine quantitative analysis, the small difference (~0.8 % of uniaxial compression) between the two types of $(2 \times x)$ superstructure is not distinguishable.

On the hexagonal Ag(111) substrate, FeO films in the one layer limit also adopt (111) crystallographic orientation. The corresponding LEED pattern exhibits well-defined moiré rosettes with little intensity scattered to the higher-order diffraction peaks, indicating that the buckling of the FeO layer is not significant. The ball model of such an overlayer is shown in Fig. 2b with a $p(9 \times 9)$ unit cell where nine lattice spacings of the substrate accommodate eight lattice spacings of the FeO film resulting in a coincidence structure. The $\left(\sqrt{91} \times \sqrt{91}\right)R5.2^{\circ}$ unit cell of FeO(111)/Pt(111) first proposed by Galloway et al. [53] is shown in Fig. 2c for comparison. The FeO(111)/Ag(111) unit cell size determined from STM and LEED measurements is ~3.25 Å, which corresponds to a surface concentration of Fe cations equal to ~79 % of the surface atom density of the Ag(111) substrate.

In Fig. 3, the reciprocal lattice of a FeO(111) layer grown on a Ag(100) surface is shown as a calculated in-plane map (panel *a*) and as an in-plane scan along the *H*-axis at $K = -1$ *RLU* and $L = 0.3$ *RLU* in the vicinity of $H = 2$ *RLU* (panel *b*). In the in-plane map the positions of the substrate crystal truncation rods (CTRs) and FeO diffraction rods are marked with red and green discs respectively, while the reciprocal unit cell of FeO(111) is indicated by the green diamonds for two rotational domains (solid and dashed lines). The unit cell of the coincidence structure is marked with black diamonds for the same domain orientations and the first-order diffraction rods originating from it are indicated with black discs and circles.

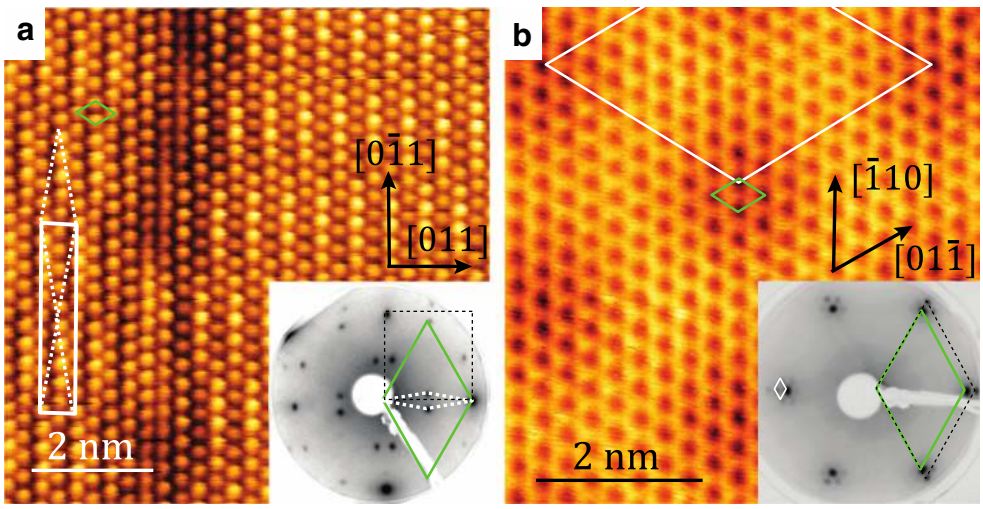

Fig. 1 **a** Atomically resolved STM (−1.0 V, 3 nA) and corresponding LEED (40 eV beam energy) images of a 0.4 ML FeO(111) film grown on Ag(100) substrate. **b** Atomically resolved STM (−0.08 V, 0.8 nA) and corresponding LEED (40 eV beam energy) images of 0.4 ML FeO(111) film grown on Ag(111) substrate

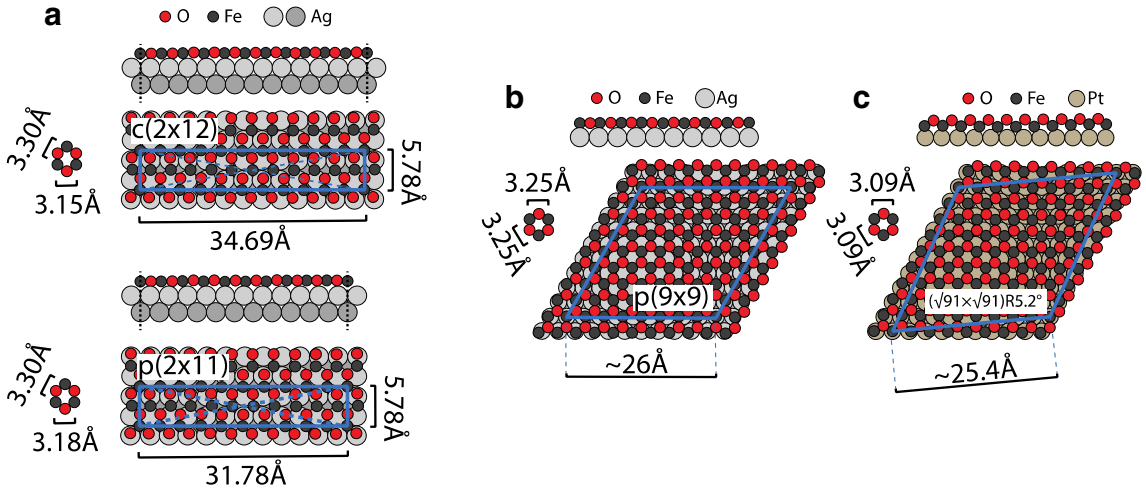

Fig. 2 Ball models of the FeO(111) monolayer **a** on Ag(100); **b** on Ag(111); **c** on Pt(111). The superstructure unit cell, its dimensions and lattice parameters are shown

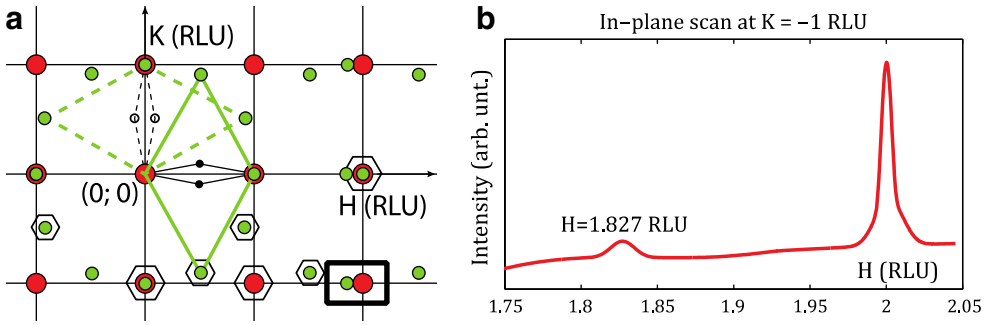

Fig. 3 **a** The part of the in-plane map of the FeO(111)/Ag(100) reciprocal lattice (*red* and *green discs* represent the positions of the diffraction rods originating from the substrate and the film respectively, *black discs* and *circles* indicate the expected positions of the first-order diffraction rods caused by the coincidence structure, *green* and *black diamonds* show the reciprocal unit cells of FeO(111) layer and the coincidence superstructure for two domain orientations (*dashed* and *solid lines*)). *Black hexagons* indicate in-plane positions of diffraction rods measured in SXRD experiments. **b** In-plane SXRD scan parallel to the H-axis at K = −1 RLU and L = 0.3 RLU with two diffraction rods indicated by the *black rectangle* in panel (**a**)

The diffraction signal from the coincidence structure, which is clearly visible in LEED (Fig. 1a) due to multiple scattering of electrons, is extremely weak and was not accessible in our SXRD experiments. The FeO(111) unit cell signal at the same time was recorded and is visible in Fig. 3b as a small peak at the $H = 1.827$ *RLU* position. A pronounced peak at $H = 2$ *RLU* corresponds to the (2; 0) CTR. Knowing the peak positions, it is possible to derive the size of the FeO unit cell to be 3.17 Å, which is in good agreement with the mean size of the unit cell along the [0-11] crystallographic direction of the substrate as determined in [33].

3.2 Out-of-Plane Geometry

We have also recorded a number of SXRD scans in out-of-plane directions following three crystal truncation rods (CTRs) originating from the substrate and four superstructure rods (SRs) containing the information about the surface structure (see Fig. 4). Their in-plane positions are marked in Fig. 3a with black hexagons. In the same image it can be seen that two CTRs – (0; −1) and (2; 0)—contain the superimposed signal coming from both bulk and surface regions while the third (1; −1) CTR is not supposed to be significantly affected by the X-ray scattering on the atoms of the FeO layer. On the other hand, the superstructure rods (two are shown in Fig. 4c, d) carry mainly the structural information about the oxide layer. The shape of the SRs is characteristic of a smooth surface without significant corrugation or roughness.

These data allow us to perform a structural determination of the surface layer. Based on the results of DFT calculations, we were able to fit the experimental data and obtain atomic coordinates (the complete list of

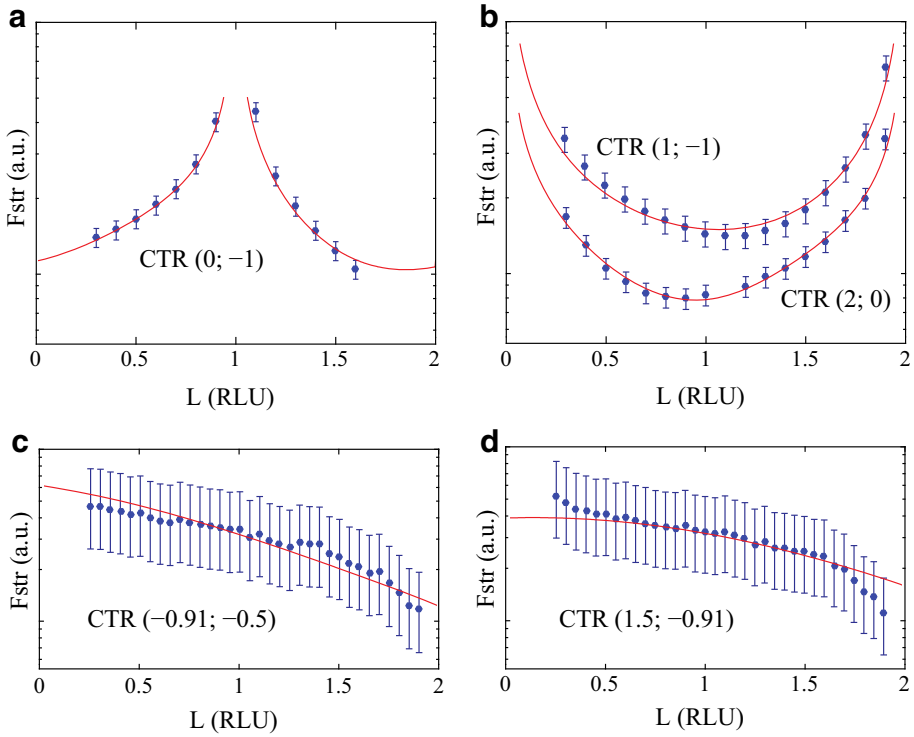

Fig. 4 Recorded SXRD data (*dots*) and fit (*curves*) for diffraction rods originating from FeO(111)/Ag(100)

experimental and theoretical atomic coordinates is available in the supplementary information, see Table S1). The systematic error of the experimental data was estimated to be equal to ∼15 % based on the difference in the structure factor of the symmetric diffraction rods. The best experimental fit was achieved in assumption of 0.56 ML FeO coverage and had the goodness, χ^2, normalized to 184 data points equal to 1.863.

The unit cell used in the theoretical calculations is a $p(2 \times 11)$. Because of its significant size, the structural relaxation was allowed only for the FeO layer while the top layers of the Ag(100) substrate were left intact. For the same reason only the interlayer distance between the bulk and the top Ag layer was varied during the fitting of experimental data. The subsequent layers of the substrate were taken into account with the unperturbed bulk structure.

Good agreement between experimental and theoretical results was achieved. The main difference is that the experimental data show a smaller distance between the FeO layer and the substrate by ∼0.25 Å and slightly bigger corrugation (by ∼0.04 Å on average) of the oxide compared to the DFT calculations (see Table S1 in the supplementary material). Additionally, the experimentally observed distance between the first and the second atomic layers of the substrate ($d_{\text{Ag top layer—bulk}}$) is larger by 0.04 Å than the interlayer distance in the bulk.

A theoretically modeled STM image of FeO(111)/Ag(100) along with the ball model of this structure are shown in Fig. 5. The STM image exhibits a mild wavy modulation of brightness in good agreement with the experimental data in Fig. 1a. Similar wavy patterns for STM images of quasi-hexagonal metal oxide monolayers grown on square substrates were reported previously in literature. For example, in [17] and [19] the authors attribute such type of pattern to relatively regular FeO(111) bilayers on Pt(100) and Pd(100) respectively with modulation of atomic positions in the direction perpendicular to the substrate surface due to the long range coincidence periodicity. Interestingly, in [54] based on the results of a thorough quantitative LEED investigation of CoO(111)/Ir(100) structure, the authors report on a drastically distorted CoO bilayer producing a similar type of STM data. In the reported model of one layer thick cobalt oxide four cobalt atoms in the unit cell are shifted towards the substrate by ∼0.5 Å while four neighboring oxygen atoms are pulled upwards by almost 1 Å relative to the average level of other atoms in the cell. During the fitting of our experimental data we considered similar atomic models for FeO(111)/Ag(100), however, they did not fit the data as well as the currently proposed model. Also, the interaction between silver and iron oxide is weaker than between iridium and cobalt oxide, which allowed us to assume a smaller distortion of the FeO layer. In addition, as discussed further below, TPD and RAIRS data show the full saturation of FeO(111)/Ag(100) with NO molecules occupying similar surface sites resulting in a (1×1) adsorbate structure, while in the case of a distorted layer a

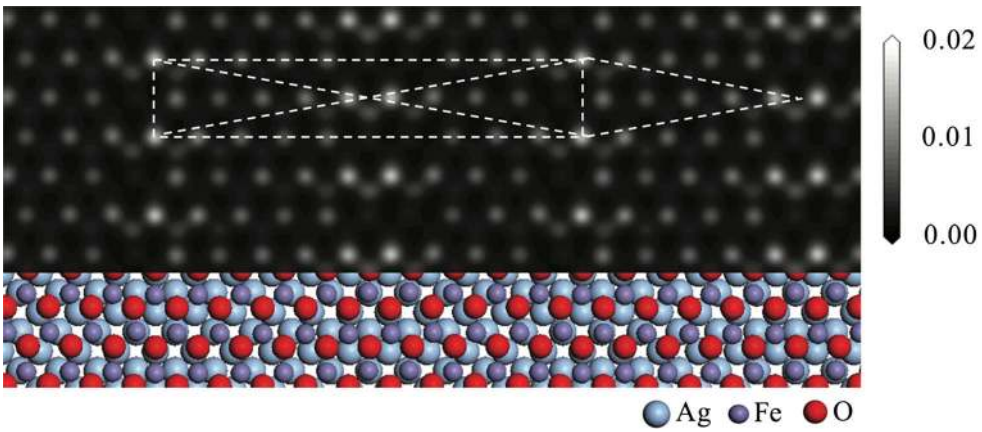

Fig. 5 Theoretically modeled STM image of FeO(111)/Ag(100) (*top*). The structural model (*bottom*). FeO unit cell is marked with the *white dashed line*

significant part of Fe atoms would likely be inaccessible for NO adsorption due to their blockage by oxygen atoms.

3.3 TPD

Figure 6a shows NO TPD spectra obtained as a function of the NO exposure to a FeO(111) layer on Ag(100) at 90 K. The curves exhibit a single distinct feature shifting from 295 to 282 K as the NO coverage increases, with saturation reached at about 2.5 Langmuir (L). The integrated TPD intensity at saturation corresponds to complete coverage of the surface with an NO molecule adsorbed on each Fe ion [52].

The results from a similar set of measurements for the FeO(111)/Ag(111) system after NO exposure at 87 K are shown in Fig. 6b. At low coverages, two peaks at ~297 and ~368 K are observed, and the peak intensities increase and shift toward lower temperature with increasing NO coverage. At saturation, the peak positions are 269 and 360 K with an additional shoulder of the major peak on the higher temperature side (~300 K) and a small broad feature at about 100 K that is attributed to NO dimers. The peak at 269 K is attributed to NO molecules adsorbed on Fe ions of the FeO layer, while the higher temperature features are assigned to different adsorption sites. Namely, it is likely that minority FeO_x domains were present on the surface, because we observe similar TPD features at 300 K and higher during measurements of NO adsorption on FeO_x films grown on Ag(111) described in [55].

3.4 RAIRS

Figure 7a shows RAIR spectra recorded for the FeO(111)/Ag(100) system at 90 K substrate temperature and different NO exposures. A single N–O stretch band is observed and blueshifts from 1798 to 1843 cm^{-1} with increasing NO coverage (the value of the N–O stretch frequency in the gas phase is 1860 cm^{-1}). A similar range of vibrational frequencies has been reported in the literature for linear iron nitrosyl compounds (Fe–N–O) [56–58]. These observations allowed us to attribute the peak in the RAIR spectra to the N–O stretch vibrations when the molecules are adsorbed vertically on Fe ions of the surface while the shift of the peak can be attributed to an increasing influence of lateral intermolecular interactions as the NO coverage increases. At saturation, NO molecules form a complete (1 × 1) monolayer with all iron ions on the surface occupied [52].

The RAIR spectra measured for NO on the FeO(111)/Ag(111) system at 87 K are shown in Fig. 5b. A single peak shifts from 1802 to 1842 cm^{-1} with increasing NO coverage, with saturation occurring at an NO dose of about 2.5 L. Similar to the RAIRS results recorded for FeO(111)/

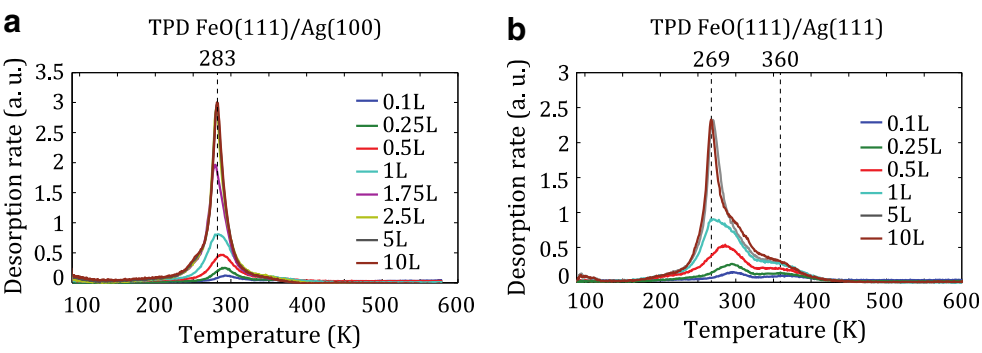

Fig. 6 TPD spectra for different NO coverage deposited **a** at 90 K on FeO(111) monolayer on Ag(100) and **b** at 87 K on FeO(111) monolayer on Ag(111)

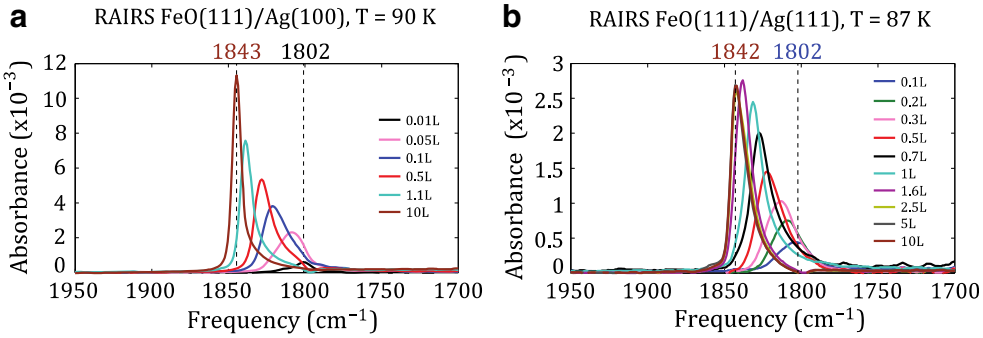

Fig. 7 RAIR spectra of NO deposited **a** at 90 K on FeO(111) monolayer on Ag(100) and **b** at 87 K on FeO(111) monolayer on Ag(111)

Ag(100), the N–O stretch band observed in this region was assigned to NO molecules that are adsorbed vertically on Fe ions of the surface.

4 Discussion

As mentioned above, the structural parameters of a one layer thick FeO film largely depend on the oxide-substrate interaction. In Table 1, the data reported in literature for stoichiometric FeO(111) monolayers grown on several different substrates are presented. The last two rows show results of our STM, LEED and SXRD investigations performed for FeO(111) on Ag(100) and Ag(111).

We used NO as a probe molecule to characterize the reactivity of FeO(111)/Ag(100) and FeO(111)/Ag(111). Summarizing the results, RAIRS and TPD data clearly show that NO readily adsorbs on both surfaces. Moreover, both TPD and RAIRS measurements reveal a single dominant feature corresponding to a preferred adsorption state that we have shown arises from NO molecules adsorbed on top of Fe ions of the surface with the molecular axis pointing upwards (see Fig. 8a, b). The saturation coverage for both surfaces is reached when every exposed Fe ion is occupied by a NO molecule, resulting in a density of the NO layers equivalent to 91 and 79 % of the surface atom densities of the Ag(100) and Ag(111) substrates, respectively.

Given the similarities in NO adsorption on the FeO(111)/Ag(100) and FeO(111)/Ag(111) structure, we conclude that the differences in the moiré pattern do not significantly influence the adsorption properties. Instead, the in-plane distance of the FeO(111) lattice, which is similar for the two Ag surfaces, determines the adsorption properties. A large in-plane distance allows the oxygen atoms to relax toward the substrate between the Fe atoms and as a result expose the Fe atoms as attractive adsorption sites for NO.

Experiments performed for FeO(111)/Pt(111) exposed to CO+NO [61] have shown that NO adsorption is negligible at temperatures near 100 K. This is in a sharp contrast with the results obtained for FeO(111) films grown on Ag

Table 1 Structural parameters obtained for FeO grown on various substrates

Substrate		FeO(111) monolayer		Coincidence structure
Material	Lattice parameter (Å)	Lattice parameter (Å)	Superstructure type	Periodicity (Å)
Cu(001) [21]	2.56	3.04	–	20.5
Cu(110) [23]	2.56	~3.05, ~3.13*	$(n \times 8)$, $n = 17$–19	43.5–48.6 × 20.5
Ru(0001) [11]	2.7	3.08	p(8 × 8)	21.6
Pd(100) [19]	2.75	3.1	c(8 × 2)	22 × 5.5
Pd(111) [14]	2.75	3.1	p(8 × 8)	22
Pt(111) [53]	2.77	3.1	$\left(\sqrt{91} \times \sqrt{91}\right)R5.2^{\circ}$	25.4
Pt(100) [17]	2.77	3.12, 3.18	p(2 × 9)	5.5 × 24.9
		3.08, 3.17	c(2 × 10)	5.5 × 27.7
Au(111) [13, 59, 60]	2.88	3.3 (±0.3)	–	34 (± 4)
Ag(111)	2.89	3.25	p(9 × 9)	26
Ag(100)	2.89	3.18, 3.30	p(2 × 11)	5.8 × 31.8
		3.15, 3.30	c(2 × 12)	5.8 × 34.7

* Stable between 950 and 1100 K

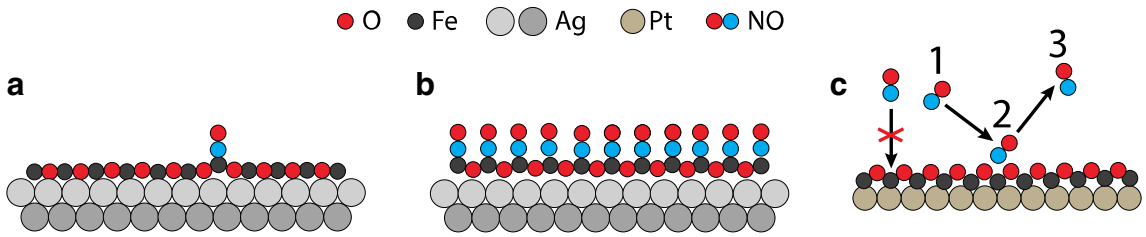

Fig. 8 Schematic side view of a low NO coverage on FeO(111)/Ag(100) (**a**), saturation NO coverage on FeO(111)/Ag(100) (**b**), NO adsorption on FeO(111)/Pt(111) hindered by protruding surface oxygen (**c**)

substrates in the present work. Merte et al. [52] provide results of DFT calculations for NO adsorption on FeO(111)/Ag(100) showing that the adsorption states are nearly electronically identical for one layer thick FeO films on Ag(100), Ag(111) and Pt(111) surfaces. The experimentally observed difference is explained by kinetic hindering of the adsorption process on FeO(111)/Pt(111) due to oxygen atoms protruding from the FeO layer and blocking access to the iron ions (see Fig. 8c). The distance between iron atoms on the surface of FeO(111)/Ag(100) is larger than for FeO(111)/Pt(111) resulting in a shift of oxygen atoms toward the substrate, which allows NO molecules to reach the exposed Fe and adsorb.

The similarity of TPD and RAIRS data for FeO(111)/Ag(100) and FeO(111)/Ag(111) along with the fact that the values of surface lattice parameters for these systems are close suggests that the same adsorption scenario holds for both silver substrates. In both cases, the substrate accommodates relatively smooth FeO(111) monolayers, which expose Fe ions to NO molecules. From Table 1, it is evident that FeO(111) films grow with smaller lateral interatomic distances on most other substrates that have been investigated. A possible exception is Au(111) where the surface unit cell might be even more expanded than for Ag(100) and Ag(111). The unit cell size reported for FeO(111)/Au(111) [13] has a large uncertainty and it is thus not entirely clear whether the FeO unit cell is larger on gold or silver. In a later publication [59], the same group reported results of water adsorption and dissociation experiments involving the same system and mentioned that the FeO(111) unit cell parameter is $\sim$3 Å and that the film is O terminated. In [60], the authors reported, however, that the unit cell size of a one monolayer thick FeO film grown on Au(111) is 3.4 $\pm$ 0.1 Å. The exact model of FeO(111)/Au(111) is, thus, still not established.

It is worth mentioning that, although the TPD and RAIR spectra of FeO(111)/Ag(100) and FeO(111)/Ag(111) are very similar, they also have some differences. The main TPD peak is at slightly lower temperature for the FeO(111) layer on Ag(111) as compared to Ag(100), suggesting a slightly weaker binding of NO on the FeO/Ag(111) structure. Since the lattice parameters of the FeO(111) monolayers on both substrates are close, the difference in NO binding energy might arise from slight differences in the electronic properties of the surfaces, caused e.g. by different film-substrate distance, and requires further investigation. The RAIRS peak at saturation is also broader for the case of FeO(111)/Ag(111), which can be connected with NO adsorption on minority FeO_x phases present within the iron oxide film where similar but not identical adsorption sites might be available. The NO stretching frequency is effectively the same for both systems, which is intriguing but not unexpected since Mehar et al. [55] have shown for different FeO_x films grown on Ag(111) that the N–O stretch band is relatively insensitive to a change in the surface binding site, i.e. there is no clear correlation between the NO binding and N–O stretching frequency.

5 Conclusions

Using STM and LEED we have shown that one monolayer of FeO grows on both Ag(100) and Ag(111) substrates with [111] crystallographic direction normal to the surface. Additionally, the surface unit cell parameter of 3.25 Å and the coincidence structure periodicity of $\sim$26 Å were found for FeO(111)/Ag(111). For the FeO(111)/Ag(100) system, the atomic coordinates of the FeO layer determined from SXRD experimental data are found to be in good agreement with theoretical calculations.

The adsorption properties of one layer thick FeO(111) films grown on Ag(100) and Ag(111) single crystals were probed using NO TPD and RAIRS and compared with data available in literature for the FeO(111)/Pt(111) system. The spectra are similar for both silver substrates and indicate that NO molecules adsorb on top of surface Fe ions with the molecular axis nominally parallel to the surface normal. The NO coverage reaches saturation when each exposed Fe ion accommodates a NO molecule. This behavior is in a sharp contrast with the negligible amount of NO adsorption reported for the FeO/Pt(111) system at 100 K. This difference has been attributed to a steric effect originating from the amount of rumpling of the FeO(111) films on Pt(111) versus the Ag surfaces. Large rumpling causes the

oxygen atoms to protrude from the surface and block access of adsorbing molecules to Fe sites in the FeO(111)/Pt(111) system. In contrast, the FeO(111) films on Ag(111) and Ag(100) are more flat and the Fe sites are thereby able to readily bind NO molecules supplied from the gas-phase. These findings demonstrate that the adsorption properties of monolayer FeO films seem to depend more strongly on the film structure compared with other characteristics of the film-substrate interaction.

Acknowledgments The authors would like to acknowledge the Röntgen-Ångström collaboration "Catalysis on the atomic scale". Financial support by the Swedish research council (VR), the Swedish Foundation for International Cooperation in Research and Higher Education (STINT) and the U.S. Department of Energy, Office of Basic Energy Sciences, Catalysis Science Division, Grant DEFG02-03ER15478 is gratefully acknowledged. The theoretical calculations were performed at C3SE (Göteborg) through a SNIC grant. We would also like to acknowledge Diamond Light Source, UK for experimental time on beamline I07 and thank Adam Warne and Matthew Forster for their help with experiments.

References

1. Chambers SA (2000) Epitaxial growth and properties of thin film oxides. Surf Sci Rep 39(5–6):105–180. doi:10.1016/S0167-5729(00)00005-4
2. Schlom DG, Haeni JH, Lettieri J, Theis CD, Tian W, Jiang JC, Pan XQ (2001) Oxide nano-engineering using MBE. Mater Sci Eng 87(3):282–291. doi:10.1016/S0921-5107(01)00726-7
3. Svetlozar S, Fortunelli A, Netzer FP (2013) Structure-property relationship and chemical aspects of oxide-metal hybrid nanostructures. Chem Rev 113(6):4314–4372. doi:10.1021/cr300307n
4. Pacchioni G (2014) Two-dimensional oxides and their role in electron transfer mechanisms with adsorbed species. Chem Rec 14:910–922. doi:10.1002/tcr.201402002
5. Parkinson GS (2016) Iron oxide surfaces. arXiv:1602.06774
6. Schoiswohl J, Sock M, Chen Q, Thornton G, Kresse G, Ramsey MG, Surnev S, Netzer FP (2007) Metal supported oxide nanostructures: model systems for advanced catalysis. Top Catal 46(1):137–149. doi:10.1007/s11244-007-0324-6
7. Freund HJ, Goodman DW (2008) Ultrathin oxide films. In: Ertl G, Knözinger H, Schüth F, Weitkamp J (eds) Handbook of heterogeneous catalysis, vol 8. Wiley-VCH, New York, pp 1309–1338
8. Nilius N (2009) Properties of oxide thin films and their adsorption behavior studied by scanning tunneling microscopy and conductance spectroscopy. Surf Sci Rep 64(12):595–659. doi:10.1016/j.surfrep.2009.07.004
9. Weiss W, Ranke W (2002) Surface chemistry and catalysis on well-defined epitaxial iron-oxide layers. Prog Surf Sci 70(1–3):1–151. doi:10.1016/S0079-6816(01)00056-9
10. Weiss W, Somorjai GA (1993) Preparation and structure of 1–8 monolayer thick epitaxial iron oxide films grown on Pt(111). J Vac Sci Technol, A 11(4):2138–2144. doi:10.1116/1.578382
11. Ketteler G, Ranke W (2003) Heteroepitaxial growth and nucleation of iron oxide films on Ru(0001). J Phys Chem B 107(18):4320–4333. doi:10.1021/jp027265f
12. Waddill GD, Ozturk O (2005) Epitaxial growth of iron oxide films on Ag(111). Surf Sci 575(1–2):35–50. doi:10.1016/j.susc.2004.10.050
13. Khan NA, Matranga C (2008) Nucleation and growth of Fe and FeO nanoparticles and films on Au(111). Surf Sci 602(4):932–942. doi:10.1016/j.susc.2007.12.027
14. Zeuthen H, Kudernatsch W, Peng G, Merte LR, Ono LK, Lammich L, Bai Y, Grabow LC, Mavrikakis M, Wendt S, Besenbacher F (2013) Structure of stoichiometric and oxygen-rich ultrathin FeO(111) films grown on Pd(111). J Phys Chem C 117(29):15155–15163. doi:10.1021/jp4042638
15. Vurens GH, Maurice V, Salmeron M, Somorjai GA (1992) Growth, structure and chemical properties of FeO overlayers on Pt(100) and Pt(111). Surf Sci 268(1):170–178. doi:10.1016/0039-6028(92)90960-E
16. Ritter M, Over H, Weiss W (1997) Structure of epitaxial iron oxide films grown on Pt(100) determined by low energy electron diffraction. Surf Sci 371(2–3):245–254. doi:10.1016/S0039-6028(96)01010-2
17. Shaikhutdinov S, Ritter M, Weiss W (2000) Hexagonal heterolayers on a square lattice: a combined STM and LEED study of FeO(111) on Pt(100). Phys Rev B 62(11):7535–7541. doi:10.1103/PhysRevB.62.7535
18. Bruns D, Kiesel I, Jentsch S, Lindemann S, Otte C, Schemme T, Kuschel T, Wollschläger J (2014) Structural analysis of FeO(111)/Ag(001): undulation of hexagonal oxide monolayers due to square lattice metal substrates. J Phys 26:315001. doi:10.1088/0953-8984/26/31/315001
19. Kuhness D, Pomp S, Mankad V, Barcaro G, Sementa L, Fortunelli A, Netzer FP, Surnev S (2016) Two-dimensional iron oxide bi-and trilayer structures on Pd(100). Surf Sci 645:13–22. doi:10.1016/j.susc.2015.10.032
20. Noguera C (2000) Polar oxide surfaces. J Phys 12:R367–R410. doi:10.1088/0953-8984/12/31/201
21. Karunamuni J, Kurtz RL, Stockbauer RL (1999) Growth of iron oxide on Cu(001) at elevated temperature. Surf Sci 442(2):223–238. doi:10.1016/S0039-6028(99)00921-8
22. Kurtz RL, Karunamuni J, Stockbauer RL (1999) Synthesis of epitaxial Fe_3O_4 films on Cu(001). Phys Rev B 60(24):R16342–R16345. doi:10.1103/PhysRevB.60.R16342
23. Pflitsch C, David R, Verheij LK, Franchy R (2001) Preparation of a well ordered iron oxide on Cu(110). Surf Sci 488(1–2):32–42. doi:10.1016/S0039-6028(01)01106-2
24. Ketteler G, Ranke W (2002) Self-assembled periodic Fe_3O_4 nanostructures in ultrathin FeO(111) films on Ru(0001). Phys Rev B 66(3):033405. doi:10.1103/PhysRevB.66.033405
25. Genuzio F, Sala A, Schmidt T, Menzel D, Freund HJ (2014) Interconversion of α-Fe_2O_3 and Fe_3O_4 thin films: mechanisms, morphology, and evidence for unexpected substrate participation. J Phys Chem C 118(50):29068–29076. doi:10.1021/jp504020a
26. Vurens GH, Salmeron M, Somorjai GA (1988) Structure, composition and chemisorption studies of thin ordered iron oxide films on platinum (111). Surf Sci 201(1–2):129–144. doi:10.1016/0039-6028(88)90602-4
27. Sun YN, Qin ZH, Lewandowski M, Carrasco E, Sterrer M, Shaikhutdinov S, Freund HJ (2009) Monolayer iron oxide film on platinum promotes low temperature CO oxidation. J Catal 266(2):359–368. doi:10.1016/j.jcat.2009.07.002
28. Sun YN, Giordano L, Goniakowski J, Lewandowski M, Qin ZH, Noguera C, Shaikhutdinov S, Pacchioni G, Freund HJ (2010) The interplay between structure and CO oxidation catalysis on metal-supported ultrathin oxide films. Angew Chem Int Ed 49(26):4418–4421. doi:10.1002/anie.201000437

29. Giordano L, Lewandowski M, Groot IMN, Sun Y-N, Goniakowski J, Noguera C, Shaikhutdinov S, Pacchioni G, Freund H-J (2010) Oxygen-induced transformations of an FeO(111) film on Pt(111): a combined DFT and STM study. J Phys Chem C 114(49):21504–21509. doi:10.1021/jp1070105
30. Fu Q, Li WX, Yao Y, Liu H, Su HY, Ma D, Gu XK, Chen L, Wang Z, Zhang H, Wang B, Bao X (2010) Interface-confined ferrous centers for catalytic oxidation. Science 328(5982):1141–1144. doi:10.1126/science.1188267
31. Zeuthen H, Kudernatsch W, Merte LR, Ono LK, Lammich L, Besenbacher F, Wendt S (2015) Unraveling the edge structures of platinum(111)-supported ultrathin FeO islands: the influence of oxidation state. ACS Nano 9(1):573–583. doi:10.1021/nn505890v
32. Kudernatsch W, Peng G, Zeuthen H, Bai Y, Merte LR, Lammich L, Besenbacher F, Mavrikakis M, Wendt S (2015) Direct visualization of catalytically active sites at the FeO–Pt(111) interface. ACS Nano 9(8):7804–7814. doi:10.1021/acsnano.5b02339
33. Merte LR, Shipilin M, Ataran S, Blomberg S, Zhang C, Mikkelsen A, Gustafson J, Lundgren E (2015) Growth of ultrathin iron oxide films on Ag(100). J Phys Chem C 119:2572–2582. doi:10.1021/jp511496w
34. Drnec J, Zhou T, Pintea S, Onderwaater W, Vlieg E, Renaud G, Felici R (2013) Integration techniques for surface X-ray diffraction data obtained with a two-dimensional detector. J Appl Crystallogr 47:365–377. doi:10.1107/S1600576713032342
35. Vlieg E (1997) Integrated intensities using a six-circle surface X-ray diffractometer. J Appl Crystallogr 30:532–543. doi:10.1107/S0021889897002537
36. Schlepütz CM, Mariager SO, Pauli SA, Feidenhans'l R, Willmott PR (2011) Angle calculations for a (2 + 3)-type diffractometer: focus on area detectors. J Appl Crystallogr 44:73–83. doi:10.1107/S0021889810048922
37. [online] http://www.esrf.eu/computing/scientific/joint_projects/ANA-ROD/
38. Kresse G, Hafner J (1993) *Ab initio* molecular dynamics for liquid metals. Phys Rev B 47(1):558–561. doi:10.1103/PhysRevB.47.558
39. Kresse G, Hafner J (1994) Ab initio molecular-dynamics simulation of the liquid-metal −amorphous-semiconductor transition in germanium. Phys Rev B 49(20):14251–14269. doi:10.1103/PhysRevB.49.14251
40. Kresse G, Furthmüller J (1996) Efficiency of ab initio total energy calculations for metals and semiconductors using a plane-wave basis set. Comput Mater Sci 6(1):15–50. doi:10.1016/0927-0256(96)00008-0
41. Kresse G, Furthmüler J (1996) Efficient iterative schemes for ab initio total-energy calculations using a plane-wave basis set. Phys Rev B 54(16):11169–11186. doi:10.1103/PhysRevB.54.11169
42. Perdew JP, Burke K, Ernzerhof M (1996) Generalized gradient approximation made simple. Phys Rev Lett 77(18):3865–3868. doi:10.1103/PhysRevLett.77.3865
43. Giordano L, Pacchioni G, Goniakowski J, Nilius N, Rienks EDL, Freund HJ (2007) Interplay between structural, magnetic, and electronic properties in a FeO/Pt(111) ultrathin film. Phys Rev B 76(7):075416. doi:10.1103/PhysRevB.76.075416
44. Monkhorst HJ, Pack JD (1976) Special points for Brillouin-zone integrations. Phys Rev B 13(12):5188–5192. doi:10.1103/PhysRevB.13.5188
45. Pack JD, Monkhorst HJ (1977) "Special points for Brillouin-zone integrations"—a reply. Phys Rev B 16(4):1748–1749. doi:10.1103/PhysRevB.16.1748
46. Tersoff J, Hamann DR (1985) Theory of the scanning tunneling microscope. Phys Rev B 31(2):805–813. doi:10.1103/PhysRevB.31.805
47. Zhang F, Li T, Pan L, Asthagiri A, Weaver JF (2014) CO oxidation on single and multilayer Pd oxides on Pd(111): mechanistic insights from RAIRS. Catal Sci Technol 4:3826–3834. doi:10.1039/c4cy00938j
48. Zhang F, Pan L, Li T, Diulus J, Asthagiri A, Weaver JF (2014) CO oxidation on PdO(101) during temperature programmed reaction spectroscopy: role of oxygen vacancies. J Phys Chem C 118:28647–28661. doi:10.1021/jp509383v
49. Brown WA, Gardner P, King DA (1995) Very-low temperature surface-reaction—N_2O formation from NO dimers at 70 to 90 K on Ag(111). J Phys Chem 99:7065–7074. doi:10.1021/j100018a045
50. Brown WA, Gardner P, Jigato MP, King DA (1995) Characterization and orientation of adsorbed NO dimers on Ag(111) at low-temperatures. J Chem Phys 102:7277–7280. doi:10.1063/1.469039
51. Brown WA, King DA (2000) NO chemisorption and reactions on metal surfaces: a new perspective. J Phys Chem B 104:2578–2595. doi:10.1021/jp9930907
52. Merte LR, Heard CJ, Zhang F, Choi J, Shipilin M, Gustafson J, Weaver JF, Grönbeck H, Lundgren E (2016) Tuning the reactivity of ultrathin oxides: NO adsorption on monolayer FeO(111). Angew Chem Int Ed. doi:10.1002/anie.201601647
53. Galloway HC, Benítez JJ, Salmeron M (1993) The structure of monolayer films of FeO on Pt(111). Surf Sci 298(1):127–133. doi:10.1016/0039-6028(93)90089-3
54. Ebensperger C, Gubo M, Meyer W, Hammer L, Heinz K (2010) Substrate-induced structural modulation of a CoO(111) bilayer on Ir(100). Phys Rev B 81(23):235405. doi:10.1103/PhysRevB.81.235405
55. Mehar V, Merte LR, Choi J, Shipilin M, Lundgren E, Weaver JF (2016) Adsorption of NO on FeO_x_ films grown on Ag(111). J Phys Chem C 120:9282–9291. doi:10.1021/acs.jpcc.6b01751
56. Ibers JA, Mingos DMP (1971) Crystal and molecular structure of hydridonitrosyltris(triphenylphosphine)iridium(I) perchlorate, $[IrH(NO)(P(C_6H_5)_3)_3][ClO_4]$. Inorg Chem 10(7):1479–1486. doi:10.1021/ic50101a033
57. Gaughan AP, Haymore BL, Ibers JA, Myers WH, Nappier TE, Meek DW (1973) Extension of the nitrosyl-aryldiazo analogy. Structure of an aryldiazo group coordinated to rhodium in a doubly bent fashion. J Am Chem Soc 95(20):6859–6861. doi:10.1021/ja00801a070
58. Haymore BL, Ibers JA (1975) Comparison of linear nitrosyl and singly bent aryldiazo complexes of ruthenium. Structures of trichloronitrosylbis(triphenylphosphine)ruthenium, $RuCl_3(NO)(P(C_6H_5)_3)_2$, and trichloro(p-tolyl)diazobis(triphenylphosphine) ruthenium-dichloromethane, $RuCl_3(p\text{-}NNC_6H_4CH_3)(P(C_6H_5)_3)_2.CH_2Cl_2$. Inorg Chem 14(12):3060–3070. doi:10.1021/ic50154a041
59. Deng X, Lee J, Wang C, Matranga C, Aksoy F, Liu Z (2011) In situ observation of water dissociation with lattice incorporation at FeO particle edges using scanning tunneling microscopy and X-ray photoelectron spectroscopy. Langmuir 27(6):2146–2149. doi:10.1021/la1049716
60. Ning Y, Wei M, Yu L, Yang F, Chang R, Liu Z, Fu Q, Bao X (2015) Nature of interface confinement effect in oxide/metal catalysts. J Phys Chem C 119(49):27556–27561. doi:10.1021/acs.jpcc.5b09498
61. Lei Y, Lewandowski M, Sun YN, Fujimori Y, Martynova Y, Groot IMN, Meyer RJ, Giordano L, Pacchioni G, Goniakowski J, Noguera C, Shaikhutdinov S, Freund HJ (2010) CO+NO versus CO+O2 Reaction on monolayer FeO(111) films on Pt(111). ChemCatChem 3(4):671–674. doi:10.1002/cctc.201000388